Accurate analytical measurements in the atomic force microscope: a microfabricated spring constant standard potentially traceable to the SI

To cite this article: Peter J Cumpson and John Hedley 2003 *Nanotechnology* **14** 1279

INSTITUTE OF PHYSICS PUBLISHING NANOTECHNOLOGY

Nanotechnology **14** (2003) 1279–1288 PII: S0957-4484(03)67223-5

Accurate analytical measurements in the atomic force microscope: a microfabricated spring constant standard potentially traceable to the SI

Peter J Cumpson[1] **and John Hedley**[2]

[1] Centre for Optical and Analytical Measurement (COAM), National Physical Laboratory, Teddington TW11 0LW, UK
[2] Institute for Nanoscale Science and Technology, University of Newcastle-upon-Tyne, NE1 7RU, UK

Received 28 July 2003, in final form 14 October 2003
Published 28 October 2003
Online at stacks.iop.org/Nano/14/1279

Abstract
Calibration of atomic force microscope (AFM) cantilevers is necessary for the measurement of nanonewton and piconewton forces, which are critical to analytical applications of AFM in the analysis of polymer surfaces, biological structures and organic molecules at nanoscale lateral resolution.

We have developed a compact and easy-to-use reference artefact for this calibration, using a method that allows traceability to the SI (Système International). Traceability is crucial to ensure that force measurements by AFM are comparable to those made by optical tweezers and other methods. The new non-contact calibration method measures the spring constant of these artefacts, by a combination of electrical measurements and Doppler velocimetry. The device was fabricated by silicon surface micromachining.

The device allows AFM cantilevers to be calibrated quite easily by the 'cantilever-on-reference' method, with our reference device having a spring constant uncertainty of around ±5% at one standard deviation. A simple substitution of the analogue velocimeter used in this work with a digital model should reduce this uncertainty to around ±2%. Both are significant improvements on current practice, and allow traceability to the SI for the first time at these nanonewton levels.

(Some figures in this article are in colour only in the electronic version)

1. Introduction

Atomic force microscopy has reached a certain level of maturity, with excellent instruments available from a number of manufacturers [1]. Atomic force microscopes (AFMs) measure displacement accurately, and can be calibrated quite easily using step-height standards, for example [2]. Some AFM instruments even incorporate laser interferometry to make traceable height measurements. The determination of the shape of the tip also has been the focus of a number of calibration methods [3–5]. The quantification of interaction forces is much more problematic [6–8]. Force on the tip is inferred from the deflection of the cantilever, using an assumed value for the cantilever spring constant. The accuracy to which the spring constant is known is the limiting factor in the accuracy of a force measurement. There is an increasing need for the accurate measurement of small forces by AFM, in the mechanical analysis of polymers [9], DNA [10], unfolding of proteins [11, 12], biological membranes [13] and ligand–receptor binding studies [14, 15]. Away from these biological applications, the technique has recently been shown [16] to be useful in the analysis of the binding of small synthetic units (specifically metallo-supramolecular systems) in studies aimed towards developing functional nanostructures. To some extent the spring constant can be calculated from the geometrical dimensions of the cantilever; however, amongst many other

factors, the functional tip coatings often used in these studies can have a significant effect on the spring constant that is difficult to model or predict [17]. A cantilever calibration method is necessary.

Many methods [6–8] have been proposed for calibrating the stiffness of an AFM probe, but none are traceable to the SI newton, and typical accuracy is only about 20–40%. Commercial reference artefacts[3] are available for AFM spring constant calibration, in the form of cantilevers of controlled dimensions. Piezoelectric transfer standards have been investigated [18]. However, they offer no traceability to the SI measurement system. This is important because there are two methods of measuring nanoscale forces that have a rapidly-increasing number of users, AFM and optical tweezers. AFM is most conveniently calibrated using reference cantilevers, whereas optical tweezer forces are estimated based on the rate of change of photon momentum caused by a beam of known intensity. Both methods are used, for example, in measuring molecular bond-breaking forces. They must both have a common force scale, or burgeoning work in both areas will be difficult to build upon.

One reason why AFM cantilevers are so difficult to make to a repeatable spring constant specification is that the thickness of AFM cantilevers is difficult to control to the tolerance required. The spring constant for cantilevers from two different batches can vary by almost a factor of two [19], because the spring constant is proportional to the cube of cantilever thickness, and the equipment for making them comes from the microelectronics industry where control of layer thickness in processing to the level of accuracy required is not a priority. This situation seems set to remain for the foreseeable future, meaning that an easy and accurate method of calibrating cantilevers would be very useful. For this reason we have previously developed a calibration reference artefact we call MARS—microfabricated array of reference springs [20, 21]. To the AFM user these are simply easy-to-use reference springs of known spring constant. An array of them allows the calibration of a wide range of AFM cantilevers with different spring constant. An example of how such a device can be used by the AFM practitioner has been described previously [20], and is shown in figure 1.

The MARS device is easy for the AFM practitioner to use, but could benefit from a method of calibration (by the manufacturer or calibration laboratory) that is traceable to the SI, i.e. to the SI unit of force, the newton. This is the aim of the work we describe here. In this paper we describe a new method of calibrating the spring constant of a MARS device *before* the cantilever measurement shown in figure 1 is carried out by the AFM practitioner.

If the problem were on a macroscopic scale, one would simply use known reference weights to give measurable deflections, and arrive at a figure for the weight per unit displacement, in newtons per metre. At micro- and nanoscales, electrical methods of generating small forces appear much more practical than methods dependent on microscopic reference weights. For example, a small capacitor may be microfabricated to apply calculable forces. Ideally one would use a capacitor geometry as independent as possible of small dimensional variations. For example, a typical microfabricated

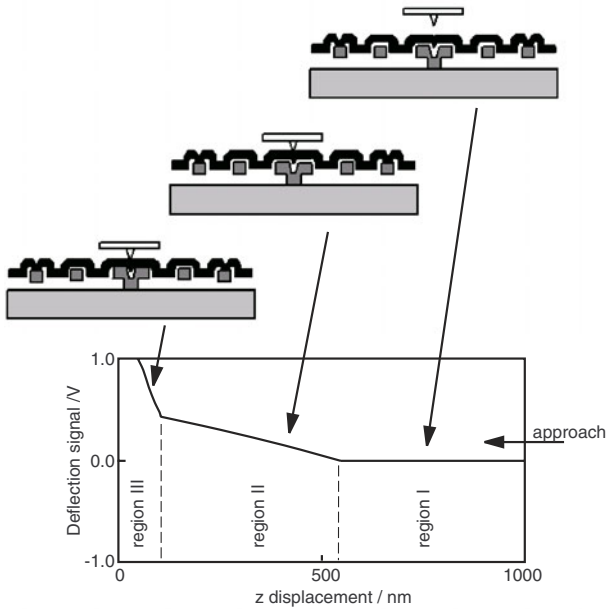

Figure 1. Experimental force–distance curve for a MARS reference spring, and three schematic cross-sectional views of the device and the AFM cantilever being calibrated. As the tip comes into contact with the device (i.e. enters region II of this plot), the slope becomes dependent on the joint spring constant of the reference spring and the AFM cantilever. In region III, the device has been pushed into contact with its base, and is essentially a hard surface. The ratio of slopes in regions II and III allows one to calculate the spring constant of the AFM cantilever with respect to the known reference device. The focus of this paper is an electrical method for measuring the spring constant of the MARS device *before* the cantilever calibration shown here.

capacitor may have a plate separation of 2.0 $\pm$ 0.2 μm. This is a percentage uncertainty of $\pm$10%, much worse than any carefully-machined macroscopic capacitor. Therefore a simple parallel-plate capacitor is probably not the best choice, since the separation of the plates may vary from one device to the next. A better method would be to use a Thompson–Lampard type calculable capacitor [22], whose change in capacitance can be theoretically related to a single length measurement. However, microfabricating a calculable capacitor to the required dimensional accuracy would be a major challenge, and the geometry of the Thompson–Lampard capacitor is not suited to common methods of microfabrication.

In the 1980s and 1990s Kibble and Robinson [23] developed a method of comparing mass standards to the SI via electrical units, known as the Watt balance method. In the Watt balance, dimensional uncertainties are eliminated from the force measurement through the combination of information from static and dynamic experiments [24], as we will describe below. The macroscopic Watt balance is a moving-coil inductive device, whereas scaling arguments suggest an electrostatic analogue would be more appropriate for microfabrication for AFM use. In fact, a large-scale capacitive analogue of the Watt balance has been constructed [25]. These Watt balances are sophisticated devices designed to achieve uncertainties of around one part in 10^8 for forces in the region of 1–10 N. This is a very demanding objective requiring metrological work of the highest order. Our application of the Watt balance principle is in an entirely different context.

[3] Veeco Metrology, Santa Barbara, USA.

A microfabricated capacitive Watt balance for AFM spring constant calibration is much simpler, due to the smaller voltages and the much lower required accuracy. The ability of the Watt balance method to eliminate uncertainties due to manufacturing dimensional tolerances is very attractive for our purposes, since microfabricated devices typically have greater percentage uncertainties in their manufactured dimensions than macroscopic machined devices. To distinguish our new microfabricated device from the macroscopic Watt balance, and from earlier MARS devices, we call it an electrical nanobalance.

The new method

The method we will describe is illustrated schematically in figure 2. The electrical nanobalance device is essentially a capacitor with one fixed electrode and one moveable electrode. The moveable electrode is suspended on a spring having a spring constant similar to that of the AFM cantilever to be calibrated. The calibration comprises three steps. Steps I and II are new, but step III comprises the 'three-region' measurement previously demonstrated for MARS devices, as shown in figure 1.

In step I, the static displacement of a moveable capacitor electrode is measured as the dc voltage applied to it is increased. In step II, a small ac 'dither' signal is added to the dc voltage to set the device into mechanical resonance, with an amplitude typically in the range 5–50 nm. We measure the small ac current through the device, and its velocity amplitude, simultaneously. The current is due to the change in capacitance that occurs as the separation of the electrodes of the capacitor varies. These steps I and II require special electrical and interferometric measurements, and will typically be performed in a calibration laboratory or National Metrology Institute such as NPL. The results of steps I and II give the spring constant of the spring supporting the moveable electrode. The electrodes of the capacitor are then permanently connected to each other electrically, and the device is sent to the AFM user. In step III this spring is then used as a reference spring within the AFM to calibrate the spring constant of the cantilever under test, without further electrical or other measurement. Step III corresponds to the process illustrated in figure 1, while steps I and II are new and described for the first time in this paper.

To the AFM user this device is simply a reference spring. The static deflection of the AFM cantilever under test is then used to measure the spring constant of that cantilever, essentially by the same method as illustrated in figure 1.

The theory and practice embodied in steps I and II are described in detail in section 3. An important point to make at this stage is that the method involves no physical contact—the calibration of the reference spring requires only electrical measurements and optical Doppler interferometry.

2. MEMS device design and fabrication

Should the device be made by conventional machining or as a MEMS (micro-electromechanical) device? MEMS design has severe restrictions imposed by the layer-wise lithographic processes commonly used, so conventional machining may seem attractive by comparison. The critical issue, however, is

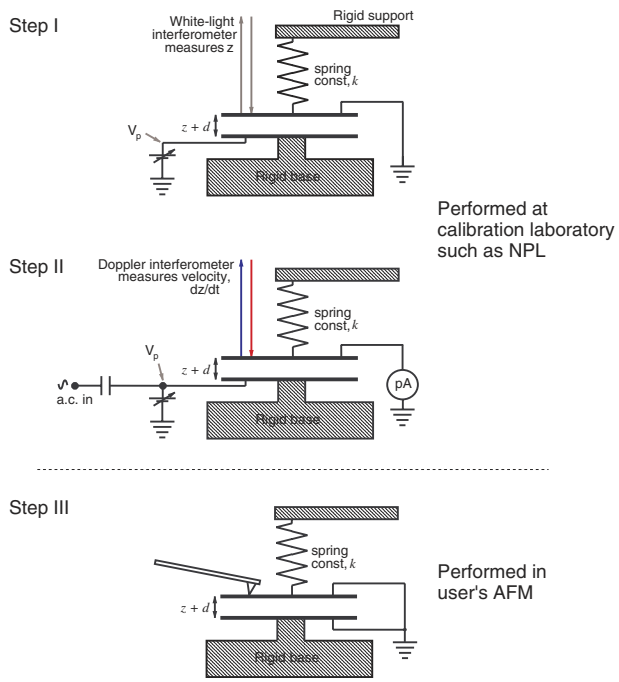

Figure 2. Schematic description of the three-step cantilever calibration method described in this work. In steps I and II, static and dynamic measurements of the displacement of a moveable capacitor electrode, together with electrical measurements, allow the spring constant of the spring supporting that moveable electrode to be measured, potentially traceably to the SI. In step III this spring is then used as a reference spring within the AFM to calibrate the spring constant of the cantilever under test, without further electrical or other measurement. Step III corresponds to the process illustrated in figure 1, while steps I and II are new and described for the first time in this paper.

the mass of the device. Conventional machining is certainly capable of producing centimetre-scale devices that can apply nanonewton forces, but they will also be susceptible to vibration due to the large ratio of their inertia to the forces they apply. Of course, careful vibration isolation can help a great deal, but often the result is a compromise in which some other aspect of performance is lost. What is more, the AFM user may well ask why they need better vibration isolation for cantilever calibration than they need for the AFM in normal use. In contrast, MEMS devices can be made extremely small, with very small mass and much lower sensitivity to vibration. Somewhat counterintuitively this leads to a much more robust device, because its small mass makes it much more resistant to damage by small mechanical shocks than the centimetre-scale version would be. We have, for example, sent such MEMS devices successfully through the postal system without problems.

Surface micromachining [26] is an attractive technology for fabrication of a electrical nanobalance device for AFM calibration, but it is capable of making only very flat structures. This makes it easy to generate small forces if one needs them to be applied in the plane of a surface-micromachined device. Electrostatic comb drives [26] are typically the method of choice, but usually operate in-plane. Instead, we need a force perpendicular to the surface for the calibration of AFM spring constants. A simple parallel-plate capacitor could be used, in

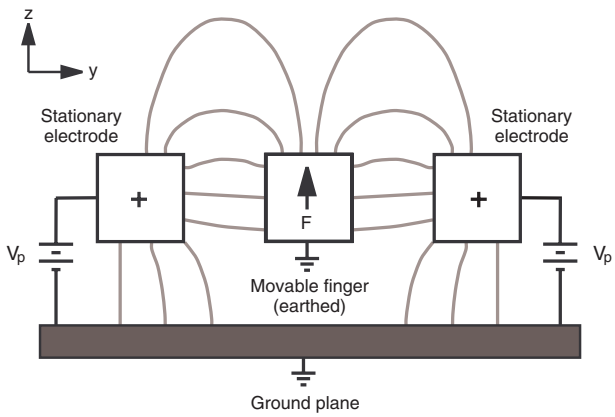

Figure 3. Levitation of the AFM landing-stage results from the asymmetry in the electric field surrounding the interdigital electrodes due to the earthed, doped polysilicon groundplane. Field lines are shown as continuous grey curves. This schematic diagram is adapted from [28].

principle, to produce a normal force. However, it is difficult to make a reliable parallel-plate capacitor that would achieve this. The large area and small separation of the capacitor plates makes these devices liable to 'stiction' [26]. What is more, there is a potential problem known in the MEMS community as 'snap-on', where the movable plate comes into contact with the fixed plate, van der Waals forces then making it almost impossible to separate them, effectively ending the useful life of the device. Ideally one would prefer a more inherently stable capacitor, for example one in which applied voltage causes the plates to separate rather than move closer together. Such a capacitor is described by Lee *et al* [27], who demonstrated a 'levitation mode' device [28]. The origin of the 'levitation' force away from the die surface is the asymmetric field distribution shown in figure 3.

We have developed a 'levitation mode' device suitable for use as the actuator in a Watt balance system. In this device an applied voltage leads to an increased separation between substrate and the AFM landing-stage, which is inherently more stable and easier to control than a simple parallel-plate capacitor. The design is illustrated in figures 4 and 5, and an optical micrograph of a completed electrical nanobalance device is shown in figure 6.

Our electrical nanobalance device incorporates a mirror on the AFM landing-stage to simplify measurement of vertical displacement and velocity by optical interferometry and Doppler velocimetry [29] respectively. The device was designed at NPL, and fabricated using the three-layer polysilicon chemical vapour deposition process. Characterization by a combination of velocimetry and interferometry was carried out at the Institute for Nanoscale Science and Technology at Newcastle University, and AFM measurements performed at NPL.

The electrical nanobalance devices we have tested resonate at around 4.3 kHz, with a full width at half maximum (FWHM) of around 7 Hz at an environmental pressure of 2.3 Pa. This corresponds to a quality factor for this resonance of $Q \approx 610$, estimated here as the ratio of the resonant frequency to the FWHM of the resonance. All measurements were performed in vacuum. Since the device has a large cross-sectional area in the direction of displacement, this quality factor is rapidly reduced by air-damping at higher pressures. Therefore the calibration of the electrical nanobalance springs must be performed in vacuum. However, this is the specialized task of the manufacturer or calibration laboratory, and the subsequent use of these springs by the AFM practitioner to calibrate AFM cantilever will typically be in air or liquid.

The electrical nanobalance device has many vibrational modes. To ensure that we attribute the correct mode of vibration to each of its resonant frequencies, measurements were made of the phase of vertical motion at a number of different points on the device. The resonance at 4.3 kHz is the fundamental vertical mode. Because the device was vibrated vertically we do not see lateral modes. The modes are very well separated in frequency so that distinguishing the fundamental mode is easy.

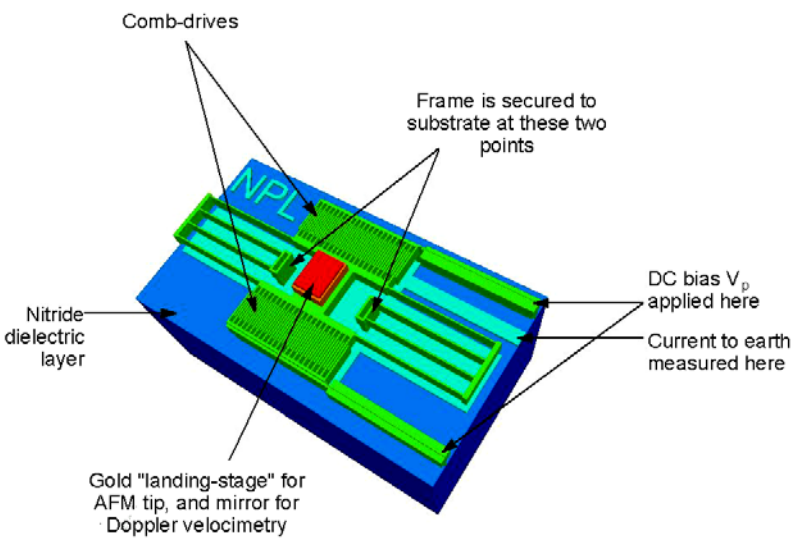

Figure 4. Three-dimensional computer model of the electrical nanobalance device. The area shown is 980 μm $\times$ 560 μm. Dimensions perpendicular to the plane have been expanded by a factor of 20 for clarity.

3. Measurements to calibrate the electrical nanobalance spring constant

In the electrical nanobalance device the most important quantity is the gradient of its capacitance as the landing-stage is displaced. If we know the gradient of its capacitance, we can calculate the force on the comb drives, and therefore the balancing mechanical force exerted by the supporting folded springs. We can measure the displacement, and so we can calculate the ratio of applied force to displacement—i.e. the spring constant. This static measurement is relatively straightforward, but we still need to measure the gradient of capacitance, since it cannot be calculated from the geometry of the device with sufficient accuracy. Indeed the constraints and relatively poor fractional dimensional accuracy of surface micromachining make this calculation more difficult and inaccurate than for many conceivable macroscopic versions. One could measure the capacitance gradient in two ways.

(i) Use a sensitive capacitance bridge to make direct measurements of the device capacitance at a number of static displacements. This would give very precise capacitance values, but would include a constant stray capacitance originating from the fixed parts of the device. To obtain the gradient of capacitance one would need to differentiate with respect to the measured displacement, increasing the uncertainty budget. Capacitance bridges have now reached such a high level of precision that this approach is viable, even for the very small capacitance of a surface micromachined capacitor.

(ii) Alternatively, one can 'dither' the displacement of the landing-stage, either mechanically (e.g. using a small piezo actuator under it) or, as we did, by superposing a very small ac drive on the dc potential applied to achieve a particular static displacement. The mechanical vibration causes a time variation in capacitance leading to a measurable ac current. By simultaneously measuring the velocity of the landing-stage one can calculate the gradient of capacitance.

The second of these two methods corresponds to the Watt balance approach. We chose this approach for use with the electrical nanobalance because

(a) one can take advantage of the sharp mechanical resonance of MEMS devices to make the 'dither' procedure distinguish very clearly between the nuisance of stray electrical capacitance and the important displacement-related capacitance gradient, and

(b) capacitance bridges of sufficient sensitivity also capable of dealing with a range of dc bias are not commercially available (though they may be very soon).

The displacement and velocity measurements were made using an instrument that has not been calibrated traceably, but comes from a class of Doppler velocimeter containing types recognized as primary methods for the measurement of velocity; Doppler velocimeters using digital demodulation are accepted for traceable primary velocity calibrations according to the appropriate ISO standard [30].

There are static and dynamic measurements to be made. Both must be performed in vacuum to avoid air-damping and to avoid attracting dust particles to critical parts of the electrostatic drive.

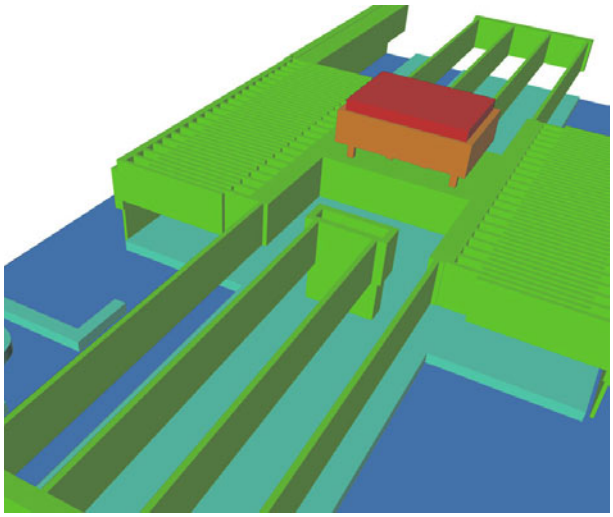

Figure 5. Close-up view centred on one of the supports of the electrical nanobalance platform. Dimensions perpendicular to the plane have again been expanded by a factor of 20 for clarity. The electrical nanobalance is a two-terminal device: the fixed outer digits of the comb drives are at a fixed potential V_p, while current to earth is measured from the structure formed by the movable frame and fixed groundplane under it, which are in electrical contact.

(1) Static measurement (shown schematically in figure 2, step I). This consists of measuring the static displacement of the AFM landing-stage as a function of applied voltage. We measured this static displacement by white-light interferometry using a Zygo NewView 5020 interferometer.

(2) Dynamic measurement (shown schematically in figure 2, step II). This consists of measuring the current to earth passing through the device, while simultaneously measuring its vibration velocity using Doppler velocimetry. The extremely sharp resonance of the platform, when operating in vacuum, allows us to separate the change in capacitance of the device due to mechanical displacement from the parasitic capacitances elsewhere in the circuit.

The current through the electrical nanobalance and the velocity of the mirror were recorded simultaneously and averaged to reduce noise using a Hewlett-Packard 3562A dynamic signal analyser. These data were then downloaded to a PC computer. Current through the electrical nanobalance was measured using a CyberAmp 320 Signal conditioner with type 403 preamplifier (Axon Instruments Inc., Union City, CA 94587, USA). By using it in 'virtual-earth' configuration, any parasitic capacitance across the input of the amplifier (or between the moving part of the actuator and the die substrate) connects virtual earth to earth, so its influence on the circuit operation is insignificant. In addition, the signal path from the electrical nanobalance was carefully surrounded on the printed circuit board (PCB) by an earthed 'guard' track, to minimize the effect of small stray currents across the bare PCB surface, for example arising from any small surface contamination by electrolytes.

We can obtain a rough estimate of the electrical nanobalance spring constant using the resonant frequency of the device and estimating its mass via the geometrical volume. The mass of the vibrating platform is estimated from its

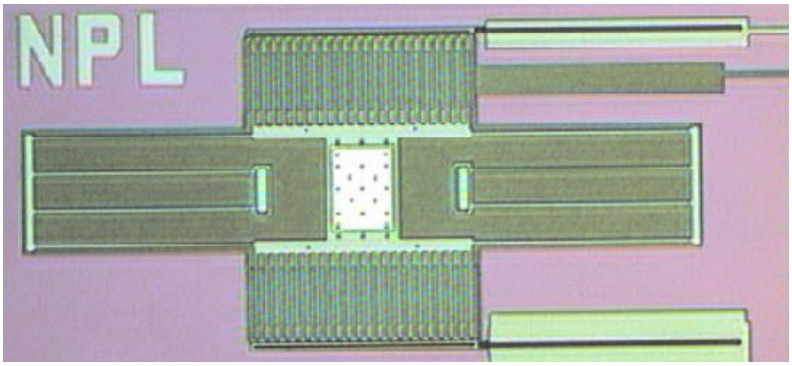

Figure 6. Optical micrograph (field of view approximately 1 mm × 0.5 mm) of the completed electrical nanobalance. Two comb drives at the top and bottom of the picture apply 'levitation mode' forces, leading to a displacement out of the plane of the photo. A folded spring mechanism provides a spring constant comparable to those of the AFM cantilevers to be calibrated. The central gold mirror can be seen clearly.

nominal dimensions at around 310±30 ng, suggesting a spring constant of $k = 0.23 \pm 0.03$ N m^{-1}.

The static deflection of the platform is the result of the balance between the elastic restoring force applied by the folded springs and the electrostatic force from the comb drives. The stored electrostatic field energy, E, is

$$E = \tfrac{1}{2} C V_{\mathrm{p}}^2 \tag{1}$$

where C is the capacitance, and V_{p} is the potential difference across it. The electrostatic force, F_{elec}, is

$$F_{\mathrm{elec}} = \frac{1}{2}\frac{\partial C}{\partial z} V_{\mathrm{p}}^2 \tag{2}$$

which balances an elastic force, F_{elastic}, of

$$F_{\mathrm{elastic}} = kz \tag{3}$$

where z is the static deflection. Figure 7 shows measurements of this static displacement z as a function of applied potential difference V_{p}. These measurements were performed in vacuum, residual pressure being measured as 2.3 Pa. These measurements correspond to step I of the process illustrated schematically in figure 2.

Now consider the dynamic part (step II) of the experiment, in which a small ac drive (in addition to the dc bias) is applied to set the platform into resonance. From elementary circuit theory, the current to earth, $i(t)$, is

$$i(t) = \frac{\mathrm{d}(CV_{\mathrm{p}})}{\mathrm{d}t}. \tag{4}$$

We now separate the capacitance of the device into two parts:

(a) the dynamic capacitance, $C(z)$, which changes as the platform is displaced, and
(b) the static or parasitic part, C_{para}; this is the capacitance between fixed parts of the device, for example adjacent tracks and pads on the silicon die.

If we measure the response of the device over a narrow frequency interval around the mechanical resonance, we expect the static capacitance to be constant, but the dynamic capacitance will vary with the motion of the platform.

$$i(t) = [C(z) + C_{\mathrm{para}}]\frac{\mathrm{d}V_{\mathrm{p}}(t)}{\mathrm{d}t} + V_{\mathrm{p}}(t)\frac{\partial C(z)}{\partial z}\frac{\mathrm{d}z}{\mathrm{d}t}. \tag{5}$$

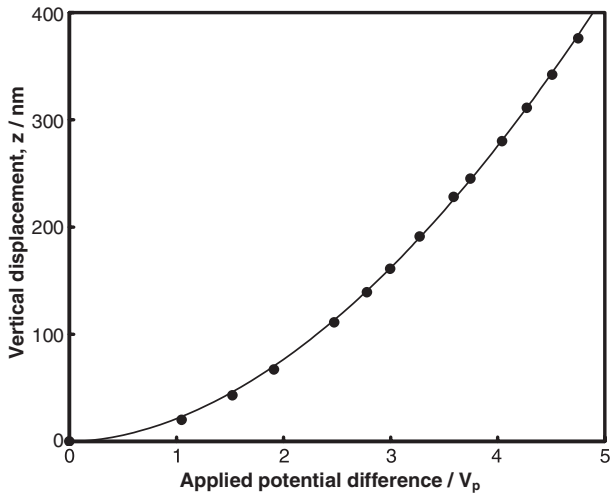

Figure 7. The vertical displacement of the electrical nanobalance platform as a function of potential applied to the fixed comb fingers. The platform is at earth potential.

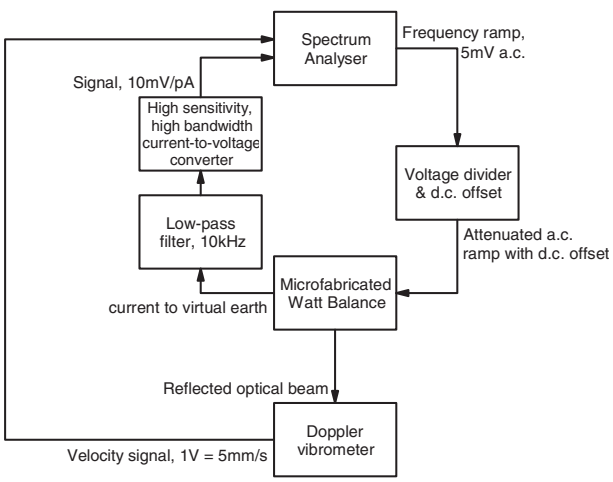

Figure 8. The arrangement for simultaneous measurement of velocity and current in the calibration of the microfabricated Watt balance (electrical nanobalance) reference springs.

We apply a dc potential of ϕ_0 to the stationary part of the comb drives, together with a small ac component $v(t)$, so that

the total voltage applied at time t is $V_p(t)$, where

$$V_p(t) = \phi_0 + v(t). \tag{6}$$

The purpose of the small ac component is to apply a small mechanical drive to the device, which, if this drive voltage is close to its mechanical resonant frequency, will cause it to vibrate mechanically with small but measurable amplitude. Typically ϕ_0 is chosen in the range 1–4 V, and $v(t)$ is a sinusoid of amplitude v_0 chosen in the range 250 μV to 2.5 mV.

$$v(t) = v_0 \sin(\omega t). \tag{7}$$

At each instant we have a measurement of the velocity $V(t) = V_0 \cos(\omega t + \theta)$ of the platform. For a given amplitude of ac drive, both the amplitude V_0 and phase with respect to that drive $(\theta - \pi/2)$ vary as the drive frequency passes through resonance. We identify the Doppler velocity with the velocity $(\mathrm{d}z/\mathrm{d}t)$ that appears in equation (5), to give

$$i(t) = [C(z)+C_{\mathrm{para}}]\frac{\mathrm{d}v(t)}{\mathrm{d}t}+[\phi_0+v_0\sin(\omega t)]\frac{\partial C(z)}{\partial z}V(t). \tag{8}$$

For a particular bias voltage ϕ_0, and an ac component amplitude v_0 sufficiently small that the capacitance $C(z)$ varies linearly over the range of mechanical vibration, we obtain

$$i(t) = [C(z) + C_{\mathrm{para}}]v_0\omega\cos(\omega t) + \phi_0\frac{\partial C(z)}{\partial z}V(t). \tag{9}$$

The arrangement used to perform these measurements is shown schematically in figure 8. The first term on the right-hand side of equation (9) represents a parasitic capacitive current that is constant in amplitude for frequencies near the mechanical resonance, and $(\pi/2)$ rad in advance of the ac drive signal. The second term is the interesting one, because it is proportional to the capacitance gradient we wish to measure. This term has the same phase as the velocity of the mirror platform (and comb drives). At low frequencies the mirror displacement is in phase with the drive signal, whereas far above the resonance it lags by π rad. Therefore the velocity is $(\pi/2)$ rad in advance of the ac drive voltage far below the resonance,

$$i(t) = [C(z) + C_{\mathrm{para}}]v_0\omega\cos(\omega t) + \phi_0\frac{\partial C(z)}{\partial z}V_0\cos(\omega t), \quad \text{for } \omega \ll \omega_r, \tag{10}$$

and lags by $\pi/2$ rad far above it,

$$i(t) = [C(z) + C_{\mathrm{para}}]v_0\omega\cos(\omega t) - \phi_0\frac{\partial C(z)}{\partial z}V_0\cos(\omega t) \quad \text{for } \omega \gg \omega_r, \tag{11}$$

where $\omega_r = 2\pi f_r$ is the angular frequency of the mechanical resonance. The sharp mechanical resonance allows us to measure the magnitude of the second term of equation (9) as this phase change occurs, since the first term is essentially constant over this narrow frequency interval.

The spectrum analyser we have is a two-channel instrument, capable of measuring the amplitude and phase of a single signal or the amplitudes of two signals simultaneously. A typical plot of the amplitude of current and velocity signals is shown in figure 9. The signal-to-noise performance of the Doppler velocimeter is particularly impressive, for maximum velocities of only around 0.8 mm s^{-1}, corresponding to a displacement amplitude of 30 nm at the top of the resonant peak.

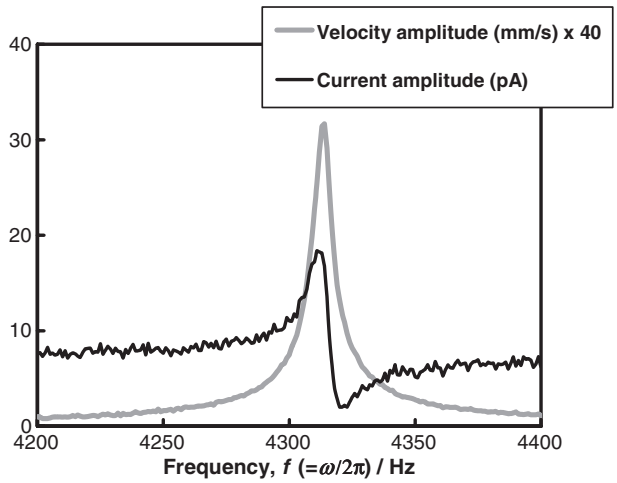

Figure 9. The measured velocity amplitude, V_0, and current amplitude, i_0, for the microfabricated Watt balance device at a dc bias of $\phi_0 = 3.0$ V.

A complete analysis has involved fitting data such as is presented in figure 9 to an electrical equivalent circuit model, for which a signal analyser with four channels would be necessary to achieve the most accurate results. However, since the resonance of this MEMS structure is so sharp, compared to the slow variation in parasitic capacitance with frequency, the transition from 'in-phase' to 'anti-phase' addition of current offers us a good way to gain insight into the measurement of the spring constant. First, combine equations (2) and (3) to give an expression for the spring constant k by balancing electrostatic and elastic forces on the platform,

$$k = \frac{\phi_0^2}{2\bar{z}}\frac{\partial C}{\partial z}, \tag{12}$$

where $\bar{z}$ is the time-average of the displacement z. Then we take the difference of equations (10) and (11) to obtain an expression for the gradient of capacitance $(\partial C/\partial z)$

$$\frac{\partial C}{\partial z} = \frac{i_0|_{\omega\gg\omega_r} - i_0|_{\omega\ll\omega_r}}{2\phi_0 V_0}, \tag{13}$$

where the current amplitudes that appear at the top right-hand side of equation (13) represent the measured current amplitude above and below resonance respectively. Using equation (13) to substitute for the capacitance gradient appearing in equation (12), we obtain

$$k = \frac{\phi_0}{4\bar{z}V_0}(i_0|_{\omega\gg\omega_r} - i_0|_{\omega\ll\omega_r}). \tag{14}$$

It is instructive to use equation (14) to construct a plot of a new quantity as a function of frequency from which the spring constant emerges naturally. We define the quantity S, where

$$S(\omega) = \frac{\phi_0[i_0(\omega) - \bar{i}_0]}{4\bar{z}V_0(\omega)} \tag{15}$$

and $\bar{i}_0$ is the average current amplitude far from resonance (we used the average of the current measured 90 Hz above the

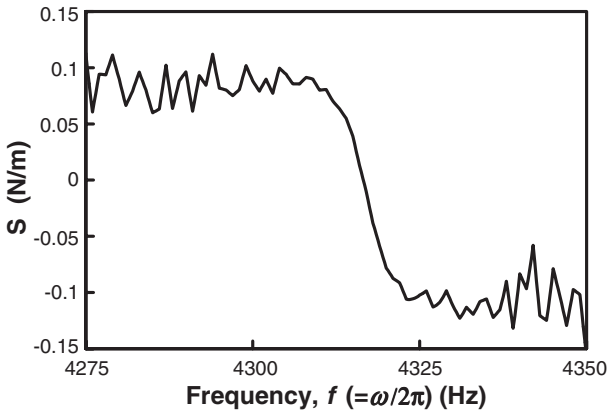

Figure 10. A plot of the ratio S against frequency in the vicinity of the mechanical resonance of the Watt balance.

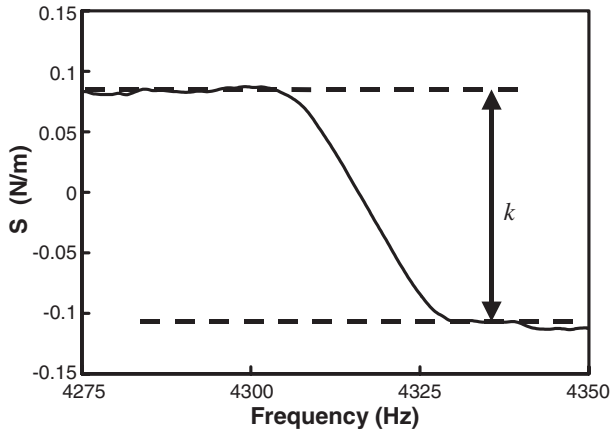

Figure 11. Data plotted in figure 10, smoothed over a 20 Hz interval. The spring constant of the device the difference in S as one passes through the resonance.

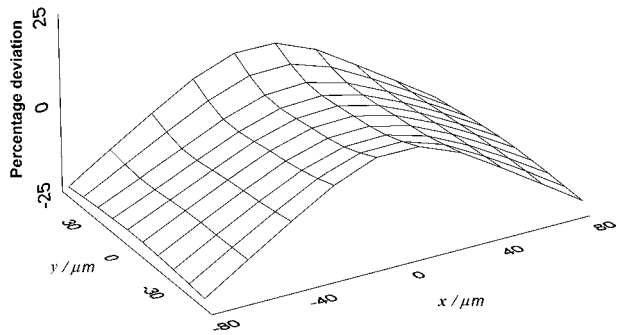

Figure 12. The percentage deviation of the effective local spring constant of the device compared to the calibrated spring constant at the centre. The x–y plane represents the surface of the electrical nanobalance landing-stage.

resonance and 90 Hz below it, in each case averaging over an interval of 10 Hz centred on ±90 Hz). The function S has no special physical interpretation, except that when plotted as a function of frequency in the vicinity of the resonance it should exhibit a step equal to the spring constant of the device. If we plot S against frequency in the region of the resonance, we should expect a sigmoidal curve of step height k, where k is the spring constant we wish to measure. Figure 10 shows these data plotted for the current and velocity measurements of figure 9. There is a good deal of residual noise that could be improved by longer acquisition times than the five seconds this scan took. A 20 Hz running average smooth improves the plot considerably, as shown in figure 11. This gives us a spring constant of 0.193 ± 0.01 N m^{-1}, in reasonable agreement with our earlier, more approximate value of 0.23 ± 0.03 N m^{-1} based on an estimate of the mass and resonant frequency of the vibrating part of the device.

One could criticize this simple analysis as 'smoothing-away' the central part of the resonant peak. In fact, this central part of the resonance (due to its greater amplitude) carries the poorest information on the gradient of capacitance, since it represents an average of this gradient over its large amplitude. The shoulders of the resonance are what is used in this plot, and carry the most useful information on the capacitance gradient averaged over an interval of only around 15 nm. Compared to the typical total displacement of the AFM tip in acquiring a force–distance curve, the shoulders are preferable to the central part of the resonance. A more rigorous fit of the data to an electrical model gives an estimate of $k = 0.195 \pm 0.01$ N m^{-1} that is not significantly more accurate.

4. Accuracy of tip placement

The electrical nanobalance offers a large AFM 'landing-stage' of 80 μm × 109 μm, so bringing the cantilever tip into contact to acquire the necessary force–distance curve is straightforward. After contact, however, the tip should be moved to the centre of the landing-stage, to avoid errors due to twisting of the folded beam springs. This can be seen clearly in figure 12, where, over the area of the landing-stage, we plot the percentage deviation of the effective local spring constant of the device compared to the calibrated spring constant at the centre. This plot was calculated by finite element analysis using the ABAQUS code within the Coventorware 2003 package[4].

The electrical nanobalance could be made easier to use by adapting the mechanical design to reduce this variation over the landing-stage, and thereby make it less necessary to move the tip to the centre before acquiring a force–distance curve. With this in mind, tripod versions of the electrical nanobalance are now being tested at NPL.

5. Testing for the absence of trapped charges

The structural material used for the electrical nanobalance is chemical vapour-deposited polycrystalline silicon. It is heavily doped to give a high conductivity, but it is conceivable that charges trapped close to its surface, perhaps at defects or grain boundaries, can add to the measured current during mechanical resonance. This would be analogous to the operation of an electret microphone, where a much greater charge on a vibrating membrane gives rise to a very easily measurable potential.

To check for the presence of trapped charges we reversed the polarity of the potential applied to the fixed section of each comb drive. As before, the moveable parts of the device are earthed. If significant trapped charges are present,

[4] Coventor, Inc., 625 Mount Auburn St., Cambridge, MA 02138, USA.

their polarity will, of course, remain the same. If so we should observe a significant change in the magnitude, not just the sign, of the measured current in the vicinity of the mechanical resonant peak in the frequency spectrum. The magnitude of this current was identical to within the experimental uncertainty for both polarities, indicating no significant contribution to the current from trapped charges. In any case, metallization of the comb drive surfaces (e.g. by gold sputter deposition) would very effectively eliminate this problem if it is observed in the future.

6. AFM cantilever calibration

We now discuss step III, as illustrated schematically in figure 2. This is the measurement of the spring constant of an AFM cantilever, k_c, by comparison with the electrical nanobalance spring constant, k. Previously [20] we have shown that for the device illustrated in figure 1, k_c can be found from the ratio of the slopes of the force–distance curve in regions II and III, as follows:

$$k_c = k\left[\frac{(\Delta V^{\mathrm{III}}_{\mathrm{A-B}}/\Delta Z^{\mathrm{III}})}{(\Delta V^{\mathrm{II}}_{\mathrm{A-B}}/\Delta Z^{\mathrm{II}})} - 1\right], \tag{16}$$

where $V_{\mathrm{A-B}}$ is a potential difference representing the 'A–B' signal from the four-quadrant detector of an AFM, and $\Delta V^{\mathrm{II}}_{\mathrm{A-B}}$, $\Delta V^{\mathrm{III}}_{\mathrm{A-B}}$ are increments in the curves in regions II and III corresponding to displacement increments of $\Delta Z^{\mathrm{II}}_{\mathrm{A-B}}$ and $\Delta Z^{\mathrm{III}}_{\mathrm{A-B}}$ in the height of the piezo stage, respectively. The ratios $(\Delta V^{\mathrm{II}}_{\mathrm{A-B}}/\Delta Z^{\mathrm{II}})$ and $(\Delta V^{\mathrm{III}}_{\mathrm{A-B}}/\Delta Z^{\mathrm{III}})$ are simply the slopes of the curve in region II (where the tip is in contact with the movable platform) and region III (where the platform is also in contact with the substrate), respectively. The spring constant of the cantilever is simply the calibrated spring constant of the reference spring multiplied by the ratio of the slope of the force–distance curve in section 3 to that in section 2, minus unity. We now have a much better reference spring than used previously [20], in that we have shown how the electrical nanobalance spring may be calibrated traceably to the SI. However, one uses it to calibrate an AFM cantilever in the same way.

A typical force–distance curve from the electrical nanobalance is shown in figure 13. This was acquired on a Park Autoprobe CP instrument (see footnote 3) at NPL, using a Micromasch 'ultrasharp' CSC-17/F5 contact cantilever pre-calibrated by the manufacturer [31]. The gold surface of the electrical nanobalance platform leads to some undesirable stick-slip structure in region II of this curve that is not present in previous polycrystalline silicon MARS devices such as that shown in figure 1. We use the retract curve here, since it is less susceptible to these events. There are now two separate points of contact of the platform with the substrate, so that two separation events (probably including a water meniscus) can be seen in the force–distance curve, separating regions II and III. These correspond to two 'dimples' [26] we designed on the underside of the platform. These structures are common in MEMS device design as a means to prevent adhesion of large parallel surfaces, and appear reproducibly in these force–distance curves as distinct separation events.

We modify equation (16) slightly to account for the angle of the AFM cantilever with respect to the electrical nanobalance platform,

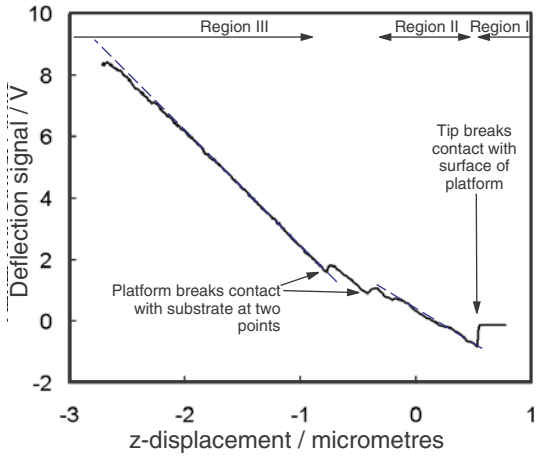

Figure 13. A typical force–distance curve for AFM calibration, as the load decreases, using the electrical nanobalance (see figure 2 step III).

$$\frac{k_c}{k} = \left[\frac{(\Delta V^{\mathrm{III}}_{\mathrm{A-B}}/\Delta Z^{\mathrm{III}})}{(\Delta V^{\mathrm{II}}_{\mathrm{A-B}}/\Delta Z^{\mathrm{II}})} - 1\right]\cos\theta, \tag{17}$$

where θ is the angle of the AFM tip with respect to the surface normal, in our case $\theta = 11°$. From the force–distance curve shown in figure 13, this gives $k_c = 0.147 \pm 0.01$ N m^{-1}, in reasonable agreement with the manufacturer's calibration value (quoted without an estimate of uncertainty) of $k_c = 0.18$ N m^{-1}. Repeating this calculation for a small number of force–distance curves acquired at similar times gives a repeatability of $\pm 3.6\%$.

We conclude with some comments concerning the practical aspects of calibrating AFM cantilever spring constants using these electrical nanobalance devices.

The experimental procedure and uncertainties involved in the 'cantilever-on-reference' method are described in detail elsewhere [6]. Although the lateral resolution of AFM is around 10 nm, it is typically very difficult to approach a target smaller than around 30 μm on a surface. This is due to the mechanics of the gross-approach mechanism of most AFM designs, relying on a stepper motor and screw thread to lower the cantilever and tube scanner. This typically has some residual eccentricity that makes precise positioning of the tip prior to contact rather difficult. The electrical nanobalance device described above has a 'landing area' of 80 μm × 109 μm. This is sufficiently large for the AFM user to approach without difficulty. Conversely, this means that the electrical nanobalance cannot be made very much smaller than these dimensions without making it significantly more difficult to use by the AFM practitioner.

The electrical nanobalance is very robust with respect to mechanical shock and vibration because of its exceptionally small inertia. However, it is just as fragile as AFM cantilevers themselves when it comes to handling—both would be destroyed if accidentally touched. In addition, the electrical nanobalance should be protected from the gross ingress of dust particles under the reference springs. We achieve this by covering the electrical nanobalance chip with a glass cover slip when not in use. The ageing properties of these devices need

to be examined, since they are fabricated in polycrystalline silicon for which ageing mechanisms that would result in a change in spring constant can be conceived. This has proven to be less of a problem than initially expected for a number of similar MEMS materials, such as in microfabricated acceleration sensors, but needs to be tested. If ageing proves to be significant compared to the other uncertainties in the calibration then a switch to a single-crystal fabrication process (such as 'silicon-on-insulator') may be necessary.

7. Conclusions

We have demonstrated a device for calibration of cantilever spring constants in atomic force microscopy, based on a calibrated reference spring that can be made traceable to the SI. We call this an *electrical nanobalance*.

(i) This particular device had a spring constant of 0.193 ± 0.01 N m^{-1}, allowing calibration of AFM cantilevers having spring constants in the range 0.03 to around 1 N m^{-1} on a wide range of AFM hardware using the 'cantilever-on-reference' method.

(ii) The uncertainty of ± 0.01 N m^{-1} seems likely to be reduced to around ± 0.003 N m^{-1} by substitution of a digital Doppler interferometry instrument.

(iii) The electrical nanobalance is straightforward to calibrate, either by an AFM manufacturer or a calibration laboratory using a combination of Doppler velocimetry and electrical current measurement.

(iv) The electrical nanobalance itself is sufficiently robust to distribute to the AFM practitioner, and large enough for the AFM practitioner to use to calibrate a wide range of cantilever types.

(v) By matching the spring constant of the electrical nanobalance to the approximate spring constant of the AFM cantilever under test, it seems straightforward to design electrical nanobalances capable of calibrating cantilevers between 0.01 and at least 90 N m^{-1} with ease.

In the future it seems likely that one could integrate the method described here into AFM cantilevers themselves. These cantilevers could have their spring constants automatically calibrated after manufacture to an uncertainty of around $\pm 2\%$ by this non-contact method.

Acknowledgments

PJC wishes to thank Dr Ian Robinson, Dr Martin Seah, Dr James Johnstone and Charles Clifford of NPL for many useful discussions and advice, Dr Ian Robinson and Dr Jonathan Williams (NPL) for advice on electrical measurement issues, Dr Joost van Kuljik (Coventor, NL) for advice on finite element meshing and Dr Jens Ebbecke (NPL) for crucial wirebonding and die packaging assistance. Particular thanks are due to Charles Clifford for acquiring the data shown in figure 13, and to Dr Martin Seah for a critical reading of the manuscript.

Microfabrication for this work was funded as part of NPL Strategic Research projects SRPQ170 and SRPQ220. This work forms part of the Valid Analytical Measurement (VAM) programme of the Department of Trade and Industry.

References

[1] Leach R K, Blunt L, Chetwynd D G and Yacoot A 2002 Nanoscience advances in the UK in support of nanotechnology *Int. J. Nanotechnol.* **1** 123–38
[2] Leach R, Haycocks J, Jackson K, Lewis A, Oldfield S and Yacoot A 2001 *Nanotechnology* **12** R1–6
[3] Villarubia J S 1994 *Surf. Sci.* **321** 287
[4] Seah M P, Spencer S J, Cumpson P J and Johnstone J E 1999 *Appl. Surf. Sci.* **144/145** 151–5
[5] Seah M P, Spencer S J, Cumpson P J and Johnstone J E 2000 *Surf. Interface Anal.* **29** 782–90
[6] Clifford C A 2003 in preparation
[7] Burnham N A, Chen X, Hodges C S, Matei G A, Thoreson E J, Roberts C J, Davies M C and Tendler S J B 2003 *Nanotechnology* **14** 1–6
[8] Myhra S 1998 *Handbook of Surface and Interface Analysis: Methods for Problem-Solving* ed J C Riviere and S Myhra (New York: Dekker)
[9] Bliznyuk V N *et al* 1998 Quantitative probing in atomic force microscopy *Scanning Probe Microscopy of Polymers* (*ACS Symposium Series* vol 694) ed B D Ratner and V V Tsukruk (Washington, DC: American Chemical Society)
[10] Clausen-Schaumann H, Rief M, Tolksdorf C and Gaub H E 2000 Mechanical stability of single DNA molecules *Biophys. J.* **78** 1997–2007
[11] Marszalek P E, Hui L, Hongbin L, Carrion-Vasquez M, Oberhauser A F, Schulten K and Fernandez J M 1999 *Nature* **402** 100–3
[12] Rief M, Gautel M, Oesterhelt F, Fernandez J M and Gaub H E 1997 *Science* **276** 1109
[13] Oesterhelt F, Oesterhelt D, Pfeiffer M, Engel A, Gaub H E and Mueller D J 2000 Unfolding pathways of individual bacteriorhodopsins *Science* **288** 143–6
[14] Willemsen O, Snel M M E, Kuipers L, Figdor C G, Greve J and DeGrooth B G 1999 A physical approach to reduce non-specific adhesion in molecular recognition atomic force microscopy *Biophys. J.* **76** 716–24
[15] Engel A, Gaub H E and Mueller D J 1999 *Curr. Biol.* **9** R133
[16] Kudera M, Eschbaumer C, Gaub H E and Schubert U S 2003 *Adv. Funct. Mater.* **13** 615–9
[17] Schwarz U D, Koster P and Wiesendanger R 1996 *Rev. Sci. Instrum.* **67** 2560
[18] Behrens I, Doering L and Peiner E 2003 *J. Micromech. Microeng.* **13** S171–7
[19] Colchero J 1998 *Procedures in Scanning Probe Microscopies* (New York: Wiley)
[20] Cumpson P J, Hedley J and Zhdan P 2003 *Nanotechnology* **14** 918–24
[21] Cumpson P J, Zhdan P and Hedley J 2003 *Ultramicroscopy SPM2003 (proceedings volume)* accepted
[22] Thompson A M and Lampard D G 1957 A new theorem in electrostatics and its application to calculable standards of capacitance *Nature* **177** 888–90
[23] Kibble B P, Robinson I A and Belliss J H 1990 *Metrologia* **27** 173–92
[24] Robinson I A and Kibble B P 1997 *IEEE Trans. Instrum. Meas.* **46** 596–600
[25] Bego V *et al* 1998 *IEEE Trans. Instrum. Meas.* **48** 212
[26] Madou M 1997 *Fundamentals of Microfabrication* (Boca Raton, FL: Chemical Rubber Company)
[27] Lee A P *et al* 1997 Electrostatic comb drive for vertical actuation *SPIE Proc.* **3224** 109
[28] Tang W C, Lim M G and Howe R T 1992 Electrostatic comb drive levitation and control method *J. Microelectromech. Syst.* **1** 170–9
[29] Hedley J, Harris A J, Burdess J S and McNie M E 2001 *SPIE Proc.* **4408** 402–8
[30] ISO 16063: 1999 Methods for the calibration of vibration and shock transducers—Part 11: primary vibration calibration by laser interferometry (Geneva: Int. Standards of Organisation)
[31] Sader J E, Chon J W M and Mulvaney P 1999 *Rev. Sci. Instrum.* **70** 3967